

Risk-Aware Autonomous Driving with Linear Temporal Logic Specifications

Shuhao Qi¹, Zengjie Zhang¹, Zhiyong Sun² and Sofie Haesaert¹

Abstract— Humans naturally balance the risks of different concerns while driving, including traffic rule violations, minor accidents, and fatalities. However, achieving the same behavior in autonomous systems remains an open problem. This paper extends a risk metric that has been verified in human-like driving studies to encompass more complex driving scenarios specified by linear temporal logic (LTL) that go beyond just collision risks. This extension incorporates the timing and severity of events into LTL specifications, thereby reflecting a human-like risk awareness. Without sacrificing expressivity for traffic rules, we adopt LTL specifications composed of safety and co-safety formulas, allowing the control synthesis problem to be reformulated as a reachability problem. By leveraging occupation measures, we formulate a linear programming (LP) problem for this LTL-based risk metric. Consequently, the synthesized policy balances different types of risks, including not only collision risks but also traffic rule violations. The effectiveness of the proposed approach is validated by three typical traffic scenarios in the Carla simulator.

I. INTRODUCTION

Developing motion planning frameworks for autonomous vehicles remains a significant challenge due to the inherent complexity and uncertainty of real-world traffic [1], [2]. The complexity arises primarily from the diverse concerns in practical driving tasks, including safety [3], traffic rules [4], and social norms [5]. The uncertainty mainly originates from the dynamic environment with unpredictable traffic participants [6] and unexpected events [7]. Taking an unprotected turn scenario in Fig. 1 as an example, the ego vehicle must make a left turn while avoiding collisions with the opponent car, obey traffic rules such as reacting to traffic lights, and follow driving norms like yielding to oncoming vehicles. Environmental uncertainty imposes the ego vehicle at the potential risk of violating the above specifications. Therefore, a risk-aware autonomous driving scheme is essential to make decisions that balance diverse risks associated with safety, traffic rules, and social norms [8].

Temporal logic provides a formal and expressive framework for describing high-level tasks that incorporate spatial and temporal constraints and synthesize provably correct controllers [9]–[11], which makes it well suited for encoding traffic tasks with rules and norms [12] and improving trustworthiness in motion planning tasks [13], [14]. While temporal logic-based planning offers significant advantages,

This work was supported by the European project SymAware under the grant No. 101070802, and by the European project COVER under the grant No. 101086228.

¹ S. Qi, Z. Zhang, S. Haesaert are with the Department of Electrical Engineering, Eindhoven University of Technology, Eindhoven, The Netherlands. {s.qi, z.zhang3, s.haeser}@tue.nl

²Z. Sun is with the College of Engineering, Peking University, Beijing, China. {zhiyong.sun@pku.edu.cn}



Fig. 1: Unprotected turn in an intersection

existing frameworks remain limited and impractical for real-world traffic deployment. Due to uncertainty and dynamic interaction in real traffic, achieving complete safety and full satisfaction of temporal logic specifications is unrealistic, making it essential to develop a risk-aware framework. Existing temporal logic planning methods quantify risk as the probability that a temporal logic specification fails and focus on maximizing the satisfaction probability of these specifications [15]–[19]. However, such risk metrics are not suitable for realistic traffic where different types of risky events may be involved [20]. In practical traffic with diverse risks, human drivers intuitively prioritize near-future and more severe events over those in the distant future or with less severity [21]. Unfortunately, the satisfaction probability of temporal logic specifications fails to differentiate the severity and timing of events [22], which results in illogical and even unsafe driving behavior.

The driver's risk field model [23], [24], proposed by the transportation community, has been shown to align with human-like risk awareness by discounting collision risks over the prediction horizon. This mode enables vehicles to track references safely by balancing risks between multiple obstacles. However, this model is limited to collision avoidance in tracking tasks, making it less effective for handling realistic traffic scenarios with complex rules. To address this, we extend the risk field model by integrating temporal logic specifications. This paper selects to use LTL [9], a classic type of temporal logic widely used in motion planning. Specifically, we extend upon the tracking task with more complex driving goals expressed by co-safe specifications and quantify risk specified as breaching safety specifications. By incorporating the inherent ability to balance timing and severity from the risk field model, this extension overcomes the limitation of temporal logic mentioned above. Safety or co-safety specifications [25] are special fragments of

LTL that can transform the control synthesis problem into a classical reachability problem. Therefore, this approach retains the ability to simplify the LTL planning into a reachability problem while preserving the necessary expressivity for traffic tasks. To formulate a tractable control synthesis problem, we rewrite the risk metric using the discounted version of occupation measures, a key concept for solving a stochastic reachability problem for a Markov Decision Process (MDP) [26]. Referring to the multi-objective control synthesis formulation for LTL in [27], we formulate a linear programming (LP) problem over product automaton to synthesize risk-aware policies using occupation measures as decision variables.

The effectiveness and scalability of the proposed method are validated in three distinct driving scenarios using the high-fidelity Carla simulator [28], demonstrating its capability to handle complexities from traffic rules and unexpected events due to uncertainty, and its scalability across versatile scenarios.

II. PRELIMINARY AND PROBLEM STATEMENT

A. Finite-State Model for Vehicles and Environments

MDP is a typical mathematical framework for decision-making in stochastic environments, and its variants, such as the partially observable MDP, can characterize more complex traffic scenarios [29]. As the first step before considering more complex models, this paper begins by using a finite-state MDP to capture the uncertain behavior of vehicles.

Definition 1. A Markov decision process (MDP) is a tuple $\mathcal{M} = (S, s_0, A, \mathbb{T})$ with S is a finite set of states and $s_0 \in S$ is an initial state; A is a finite set of actions; and $\mathbb{T}: S \times A \times S \rightarrow [0, 1]$ is a probabilistic transition kernel. \square

We denote a finite path of \mathcal{M} as $\mathbf{s}_n := s_0 a_0 \dots a_{n-1} s_n$, $n \in \mathbb{N}$, where $s_i \in S$ and $a_i \in A$ for all $i \leq n$. Similarly, we denote an infinite paths as $\mathbf{s} = s_0 a_0 s_1 a_1 \dots$. The inputs of \mathcal{M} are selected according to a policy defined as follows.

Definition 2. A policy is a sequence $\pi := \pi_0 \pi_1 \pi_2 \dots$ of stochastic kernels $\pi_n: H \times A \rightarrow [0, 1]$, where H denotes the collection of all the finite paths \mathbf{s}_n . The set of all policies is denoted by Π .

Given a policy $\pi \in \Pi$ and a finite path \mathbf{s}_n , the distribution of the next control input a_n is given by $\pi_n(\cdot | \mathbf{s}_n)$ with $\sum_{a_n} \pi_n(a_n | \mathbf{s}_n) = 1$. Given the initial state s_0 , the stochastic kernel $s_{n+1} \sim \mathbb{T}(\cdot | s_n, a_n)$ together with the policy $a_n \sim \pi_n(\cdot | \mathbf{s}_n)$ induce a unique probability distribution over the paths of \mathcal{M} , which we denote by \mathbb{P}_π . Policies that depend on \mathbf{s}_n only through the current state s_n are called *Markov policies*, which means $\pi_n: S \times A \rightarrow [0, 1]$. A Markov policy is called stationary if the kernels π_n do not depend on the time index n . When it is applied to the MDP, the resulting model is called a Markov Chain (MC), defined as follows,

Definition 3. A Markov Chain (MC) is defined as a tuple $\mathcal{C} = (S, s_0, \mathbb{T})$ where S and s_0 are defined as in the MDP, and $\mathbb{T}: S \times S \rightarrow [0, 1]$ is a probabilistic transition kernel. \square

Since environmental states are uncontrollable, an MC is used to represent the evolution of environments [30]. In summary, an MDP, denoted by $\mathcal{M}_v = (S_v, s_v^0, A, \mathbb{T}_v)$, is used to represent the behavior of the ego vehicle, while an MC model, denoted by $\mathcal{C}_e = (S_e, s_e^0, \mathbb{T}_e)$, captures the behavior of the environment. Furthermore, the composition of \mathcal{M}_v and \mathcal{C}_e forms a new MDP model, defined as $\mathcal{M} = (\bar{S}, \bar{s}_0, A, \bar{\mathbb{T}})$, where $\bar{S} := S_v \times S_e$, $\bar{s}_0 = (s_v^0, s_e^0)$, and $\bar{\mathbb{T}}: \bar{S} \times A \times \bar{S} \rightarrow [0, 1]$ based on $\bar{\mathbb{T}}(\bar{s}, a, \bar{s}') = \mathbb{T}_v(s_v, a, s'_v) \times \mathbb{T}_e(s_e, s'_e)$.

B. Specifications: Linear Temporal Logic (LTL)

The set of atomic propositions $AP = \{p_1, \dots, p_n\}$ defines an alphabet $\Sigma := 2^{AP}$, where each letter $\omega \in \Sigma$ contains the set of atomic propositions that are true. A labeling function \mathcal{L} maps states to letters in the alphabet Σ , such that an infinite path $\mathbf{s} = s_0 s_1 s_2 \dots$ generates a word as $\omega := \mathcal{L}(s_0) \mathcal{L}(s_1) \mathcal{L}(s_2) \dots$. A suffix of a word ω is $\omega_k = \omega_k \omega_{k+1} \omega_{k+2} \dots$, where $\omega_i \in \Sigma$ and $k \in \mathbb{N}_{\geq 0}$.

Syntax: An LTL [9] specification is recursively defined as,

$$\psi ::= \top \mid p \mid \neg \psi \mid \psi_1 \wedge \psi_2 \mid \bigcirc \psi \mid \psi_1 \mathbf{U} \psi_2, \quad (1)$$

where ψ_1, ψ_2 and ψ are LTL formulas, $p \in AP$ is an atomic proposition, \neg is the *negation* operator, \wedge is the *conjunction* operator that connects two LTL formulas, and \bigcirc and \mathbf{U} represent the *next* and *until* temporal operators, respectively. Other logical and temporal operators, namely *disjunction* \vee , *implication* \rightarrow , *eventually* \lozenge , and *always* \square can be defined as, $\psi_1 \vee \psi_2 := \neg(\neg \psi_1 \wedge \neg \psi_2)$, $\psi_1 \rightarrow \psi_2 := \neg \psi_1 \vee \psi_2$, $\lozenge \psi := \top \mathbf{U} \psi$, and $\square \psi := \neg \lozenge \neg \psi$.

Semantics: For a given word ω , basic semantics of LTL are given as $\omega_k \models p$, if $p \in \omega_k$; $\omega_k \models \neg p$, if $p \notin \omega_k$; $\omega_k \models \psi_1 \wedge \psi_2$, if $\omega_k \models \psi_1$ and $\omega_k \models \psi_2$; $\omega_k \models \bigcirc \psi$, if $\omega_{k+1} \models \psi$; $\omega_k \models \psi_1 \mathbf{U} \psi_2$, if $\exists i \in \mathbb{N}$ such that $\omega_{k+i} \models \psi_2$, and $\omega_{k+j} \models \psi_1$ holds $\forall 0 \leq j < i$.

Fragments: Two notable fragments of LTL are the safety and co-safety specifications [25], which allows reasoning about the satisfaction of an infinite word using only a finite prefix. Specifically, a co-safety formula is satisfied if there exists a finite “good” prefix regardless of any infinite suffix. Conversely, the violation of a safety specification depends on the existence of a finite bad prefix. In other words, safety fragments represent “bad thing never happens”, while co-safety fragments depict “good thing eventually happens”. A syntactically co-safety LTL (scLTL) formula ψ over a set of atomic propositions AP is recursively defined as,

$$\psi ::= \text{true} \mid p \mid \neg p \mid \psi_1 \wedge \psi_2 \mid \psi_1 \vee \psi_2 \mid \bigcirc \psi \mid \psi_1 \mathbf{U} \psi_2$$

where ψ_1, ψ_2 , and ψ are scLTL formulas, and $p \in AP$. An LTL formula, ψ , is a safety specification if and only if its negation $\neg \psi$ is a co-safety specification.

Automaton: A general LTL specification can be translated into a Büchi automaton [9] whose semantics are defined over infinite words. In contrast, scLTL and safety specification can be also translated into deterministic finite-state automata (DFA), defined as follows.

Definition 4. An DFA is a tuple $\mathcal{A} = (Q, q_0, \Sigma, \delta, F)$, where Q is a finite set of states and $q_0 \in Q$ is an initial state; Σ

is a finite input alphabet; $\delta : Q \times \Sigma \rightarrow Q$ is a deterministic transition function; $F \subset Q$ is a set of final states. \square

Final states are sink states, i.e., a path entering it stays there forever. The final states in the DFA from a co-safety specification are accepting states, while the final states in the DFA of a safety specification are non-accepting.

Study Case: In an intersection scenario depicted in Fig. 1, the ego vehicle is expected to eventually reach a target area labeled “ t ”, avoid collisions with the other vehicle labeled “ v ”, refrain from entering non-drivable areas labeled “ n ”, and also wait for a green light event labeled “ g ” before entering the intersection area labeled “ i ”. In this scenario, the LTL specification is $\psi = \psi_{cs} \wedge \psi_s$ with a co-safety formula $\psi_{cs} = \Diamond(t)$ and a safety formula $\psi_s = \Box(\neg g \rightarrow \neg i) \wedge \Box(\neg n \wedge \neg v)$, defined over $AP = \{t, v, g, i\}$. DFAs can be autonomously translated from ψ_s and ψ_{cs} using off-the-shelf toolboxes [31].

C. Risk-Aware Control Synthesis Problem

Since traffic rules are primarily concerned with the occurrence of good or bad events rather than repetitive behaviors, we use the combination of safety and co-safety fragments to effectively represent nearly all traffic tasks and rules while mitigating the computational demand of control synthesis. Thus, we consider an LTL specification in the form of $\psi = \psi_{cs} \wedge \psi_s$ defined over an atomic proposition set AP , composed with a safety formula ψ_s and a co-safety formula ψ_{cs} . The corresponding DFAs of ψ_{cs} and ψ_s are denoted by \mathcal{A}_{cs} and \mathcal{A}_s , respectively. To represent the uncertain behavior of both the environment and vehicle, we use a composed MDP $\overline{\mathcal{M}}$, as defined in Definition 1. This composed MDP combines an MDP model for an ego vehicle, \mathcal{M}_v defined in Def. 1, and an MC model for an uncontrollable environment, \mathcal{C}_e defined in Definition 3. The states of $\overline{\mathcal{M}}$ are labeled by \mathcal{L} to an alphabet set Σ , which can be used to verify the satisfaction of ψ . To handle the uncertainty in realistic traffic like a human driver, we aim to develop a human-like risk metric for ψ and then synthesize a stochastic policy $\pi \in \Pi$ that respects a human-like risk metric.

III. HUMAN-LIKE RISK METRIC

Risk metrics are often defined based on simple reach-avoid problems [32]. Therefore, we will start by rewriting the satisfaction problem for the given specifications $\psi = \psi_{cs} \wedge \psi_s$ as a reach-avoid problem over product MDP.

A. Product MDP and Reachability Problem

Definition 5. The product MDP of $\overline{\mathcal{M}}$, \mathcal{A}_{cs} and \mathcal{A}_s is defined as a tuple $\mathcal{P} = (Z, z_0, A, \hat{\mathbb{T}}, G, D)$, with the state set $Z := S \times Q_{cs} \times Q_s$, the action set A , and the initial state $z_0 = (\bar{s}_0, \delta_{cs}(q_{cs}^0, \mathcal{L}(\bar{s}_0)), \delta_s(q_s^0, \mathcal{L}(\bar{s}_0)))$. $\hat{\mathbb{T}} : Z \times A \times Z \rightarrow [0, 1]$ is the probabilistic transition kernel, which can specify a transition from state $z_n = (\bar{s}_n, q_s^n, q_{cs}^n)$ to $z_{n+1} = (\bar{s}_{n+1}, q_s^{n+1}, q_{cs}^{n+1})$ under action $a_n \in A$ based on $\bar{s}_{n+1} \sim \hat{\mathbb{T}}(\cdot | \bar{s}_n, a_n)$, $q_{cs}^{n+1} = \delta_{cs}(q_{cs}^n, \mathcal{L}(\bar{s}_n))$ and $q_s^{n+1} = \delta_s(q_s^n, \mathcal{L}(\bar{s}_n))$ for each $n \in \mathbb{N}$. Denote the accepting set for ψ_{cs} as $G := \bar{S} \times F_{cs}$, and the non-accepting set for ψ_s as $D := \bar{S} \times F_s$.

It is well known [9] that the satisfaction probability of co-safety specification equates to a reachability probability towards the accepting state set of the product automaton defined in Def. 5,

$$\mathbb{P}_\pi(\omega \models \psi_{cs}) = \bar{\mathbb{P}}_{\bar{\pi}}(\Diamond G) = \mathbb{E}_{\bar{\pi}} [\sum_t^\infty \mathbf{1}(z_t \in G)], \quad (2)$$

where $\mathbf{1}(\cdot)$ is an indicator function, $\bar{\pi}$ is policy for \mathcal{P} , and $\bar{\mathbb{P}}_{\bar{\pi}}$ denotes the probability distribution over the paths of \mathcal{P} under $\bar{\pi}$. Note that $\bar{\pi}$ for \mathcal{P} that is a Markovian and stationary policy, which is converted from π for \mathcal{M}_v defined in Def. 2. Similarly, for every safety specification ψ_s , the violation probability equates to a reachability probability towards the non-accepting state set of \mathcal{P} ,

$$\mathbb{P}_\pi(\omega \not\models \psi_s) = \bar{\mathbb{P}}_{\bar{\pi}}(\Diamond D) = \mathbb{E}_{\bar{\pi}} [\sum_t^\infty \mathbf{1}(z_t \in D)]. \quad (3)$$

B. Limitations of Event Probability

Using satisfaction and violation probability defined in (2) and (3) to evaluate safety in realistic traffic might lead to unnatural behavior. The event probability in (2) and (3) means that each possible trace generated by π that drives \mathcal{P} to enter into final states in finite time gets weight 1 and all else gets weighted 0, which is displayed in Fig. 2. Such an approach embraces two points against the awareness way of human drivers: (1) It does not account for the timing of violations, which may cause the vehicle to react too early to dangers that happen in the distant future; (2) It fails to consider varying costs associated with various types of violations, preventing the vehicle from appropriately balancing the seriousness of various dangers. Thus, a risk metric reflecting human-like risk awareness is necessary.

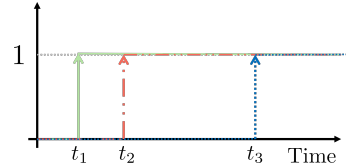


Fig. 2: Sketch for \mathbb{P}_π with three traces in different colors.

C. Human-like Metric Design

Discounted rewards are commonly used in reinforcement learning and economics to account for the timing of events when decisions lead to rewards at different moments in the future. The satisfaction probability, $\mathbb{P}_\pi(\omega \models \psi_{cs})$, can be modified by introducing discounting as follows,

$$\bar{\mathbb{P}}_{\bar{\pi}} = \mathbb{E}_{\bar{\pi}} [\sum_t^\infty \gamma^t \mathbf{1}(z_t \in G)], \quad (4)$$

where $\gamma < 1$ is a discount factor. This discounting represents the preference of people for obtaining rewards sooner rather than later. The rationality of the discounting operation has also been supported by psychology studies [33]. When it comes to violation risks of safety specification, we propose a similar metric. In addition, varying severity of events are considered by a cost mapping function, denoted as $c(\cdot) : Z \rightarrow \mathbb{R}$, that assigns cost values to different product states. Specifically, $c(\hat{z}) = 0$ if $\hat{z} \notin D$, while $c(\hat{z}) > 0$ if $\hat{z} \in D$.

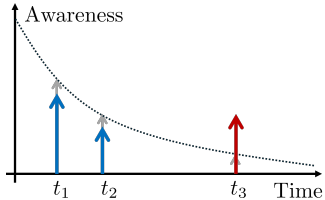


Fig. 3: Sketch for $\mathcal{R}_{\bar{\pi}}$. The grey arrows indicate the awareness levels assigned to violation events, while the colored arrows represent the corresponding risk values. Red and blue colors differentiate between two different types of events.

Furthermore, we propose the following metric to evaluate the risk of a policy π ,

$$\mathcal{R}_{\bar{\pi}} = \mathbb{E}_{\bar{\pi}} [\sum_t^{\infty} \gamma^t c(z_t)]. \quad (5)$$

The proposed metric addresses the limitations of event probabilities. As depicted in Fig. 3, discounting reflects how a driver's awareness gradually decreases over time, causing the perceived risk for the same event to decrease accordingly. When an event is significantly severe, like the one indicated by the red arrow, the risk metric in (5) places greater importance on this event than on less severe ones. Therefore, this metric can account for both the timing and severity of risky events. Defined over product state space, this metric can be seen as an extension of the driver's risk field (DRF) model [23], [24] to LTL specifications.

Driver's Risk Field (DRF) model is designed empirically to evaluate the uncertainty distribution from a driver's view. The risk field $\alpha(\cdot) : \mathbb{R}^2 \rightarrow \mathbb{R}$ maps horizontal coordinates to scalar values representing the driver's attention. To model human-like awareness, DRF is designed based on the intuition that the importance of future events diminishes while the corresponding uncertainty increases along the predictive horizon. A detailed formulation of DRF can be found in [23]. Perceived risk is evaluated by calculating the expected event cost, which is the product of the risk field and the cost map. With a grid discretization, the DRF risk metric is defined as:

$$\mathcal{R} = \sum_{x \in X} \sum_{y \in Y} c(x, y) \alpha(x, y), \quad (6)$$

where $c(\cdot) : \mathbb{R}^2 \rightarrow \mathbb{R}$ represents the cost distribution over horizontal coordinates, and X and Y are finite sets of discretized coordinates along with x and y -axis.

Inspired by DRF risk metric in Eq. (6), the risk metric in Eq. (5) is rewritten as follows:

$$\begin{aligned} \mathcal{R}_{\bar{\pi}} &= \mathbb{E}_{\bar{\pi}} [\sum_t^{\infty} \sum_{z \in Z} \gamma^t c(z) \mathbf{1}(z_t = z)] \\ &= \sum_{z \in Z} c(z) \underbrace{\mathbb{E}_{\bar{\pi}} [\sum_t^{\infty} \gamma^t \mathbf{1}(z_t = z)]}_{\beta_{\bar{\pi}}(z)}. \end{aligned} \quad (7)$$

Referring to the standard occupation measure formulated as $\mathbb{E}_{\bar{\pi}} [\sum_t^{\infty} \mathbf{1}(z_t = z)]$, $\beta_{\bar{\pi}}(z)$ can be regarded as a discounted version of the occupation measure. An occupation measure describes the expected number of times that a state has been visited before reaching the final set, given a Markov

and stationary policy $\bar{\pi}(z, a)$. Occupation measures can be used to formulate stochastic shortest path problems [34]. By comparing risk metrics in (7) and (6), it is evident that the discounted occupation measure plays a similar role as the DRF model. In addition, the discounted occupation measure embraces similar awareness for events as the DRF model. Thus, we conjecture that the proposed risk metric embodies a similar human-like risk awareness as DRF.

IV. RISK-AWARE CONTROL

In this section, we formulate a first risk-aware control synthesis problem with the proposed metrics. A reasonable approach is to maximize the rewards metric of co-safety specification and also keep the risk metric of safety specification in an acceptable range, which is formulated as follows,

$$\max_{\bar{\pi}} \mathcal{V}_{\bar{\pi}} (\omega \models \psi_{cs}) \text{ s.t. } \mathcal{R}_{\bar{\pi}} (\omega \models \psi_s) \leq r_{th}, \quad (8)$$

where $r_{th} \in \mathbb{R}$ is a constant threshold. We first reformulate this optimization problem into a linear programming problem. Afterward, we detail how traffic rules and vehicle dynamics should be integrated and evaluate the risk metric in a traffic scenario.

A. Linear Programming Problem

This problem can be formulated with discounted occupation measures defined over the product MDP, \mathcal{P} . Firstly, the discounted occupation measures with respect to product states, denoted by $\beta_{\bar{\pi}}(z)$, equates to the sum of the discounted occupation measure with respect to state-action pairs, denoted by $\beta_{\bar{\pi}}(z, a)$, over action set A , i.e., $\beta_{\bar{\pi}}(z) = \sum_{a \in A} \beta_{\bar{\pi}}(z, a)$. Specifically, $\beta_{\bar{\pi}}(z, a)$ is defined as,

$$\beta_{\bar{\pi}}(z, a) := \mathbb{E}_{\bar{\pi}} [\sum_{t=0}^{\infty} \gamma^t \mathbf{1}(z_t = z, a_t = a)]. \quad (9)$$

For any $z' \in Z$, the occupation measure at state z' should satisfy the balance constraint to ensure the equivalence between the incoming transitions and the initial state distribution with the occupation measure at z' ,

$$\beta_{\bar{\pi}}(z') = \sum_{z \in Z} \sum_{a \in A} \beta_{\bar{\pi}}(z, a) \hat{\mathbb{T}}(z, a, z') + \mathbf{1}(z' = z_0), \quad (10)$$

A solution to this balance equation gives a stationary policy,

$$\bar{\pi}(z, a) = \frac{\beta_{\bar{\pi}}(z, a)}{\sum_{a \in A} \beta_{\bar{\pi}}(z, a)} = \frac{\beta_{\bar{\pi}}(z, a)}{\beta_{\bar{\pi}}(z)}. \quad (11)$$

For this policy, the reward metric for co-safety formula ψ_{cs} is formulated with discounted occupation measures as,

$$\bar{\mathcal{V}}_{\bar{\pi}}(\Diamond G) = \sum_{z' \in G} \sum_{z \in Z} \sum_{a \in A} \beta_{\bar{\pi}}(z, a) \hat{\mathbb{T}}(z, a, z') + \mathbf{1}(z_0 \in G). \quad (12)$$

To sum up, the policy, reward metric, and risk metric are formulated with occupation measures in (11), (12) and (7), respectively. Furthermore, the control synthesis problem in (8) can be formulated as a linear programming problem

using $\beta_{\bar{\pi}}(z, a) \geq 0$ for all $(z, a) \in Z \times A$ as decision variables,

$$\begin{aligned} \max_{\{\beta_{\bar{\pi}}(z, a)\}} \quad & \bar{V}_{\bar{\pi}}(\Diamond G) \\ \text{s.t.} \quad & \sum_{z \in Z} \sum_{a \in A} c(z) \beta_{\bar{\pi}}(z, a) \leq r_{th} \\ & \beta_{\bar{\pi}}(z, a) \geq 0, \forall (z, a) \in Z \times A \\ & \beta_{\bar{\pi}}(z') = (10), \forall z' \in Z \end{aligned} \quad (13)$$

The optimal policy $\bar{\pi}$ can be extracted from the optimized occupation measures using Eq. (11), and then $\bar{\pi}$ can convert to $\pi \in \Pi$ defined on \mathcal{M}_v . This LP problem can be solved using an off-the-shelf solver, Gurobi [35].

To visualize the risk field calculated by the LP problem intuitively, we first consider a reach-avoid problem over the 2-dimensional positions of the ego vehicle, excluding the product states that include environment states and specification automaton states. Fig. 4 displays the risk field with discounted occupation measures obtained by solving the LP problem in Eq. (13). The red solid line represents the optimal path determined by the optimized risk field. As shown in the figure, we can see that the risk field obtained by the occupation measure aligns with the pattern of the proposed risk field in [23], revealing the underlying equivalence between the proposed metric and DRF. In addition, the different risk thresholds r_{th} in Eq. (13) will alter the shape of the risk field and further tune the conservatism of the generated policy.

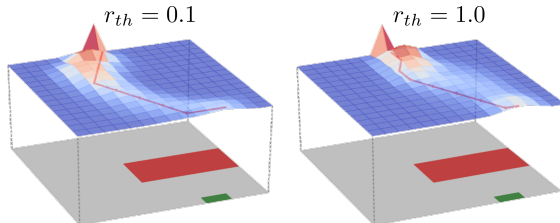


Fig. 4: Risk field extracted from discounted occupation measures. The higher layer is the risk field, while the lower layer is a map of a reach-avoid problem, where the red rectangle is an obstacle and the green rectangle is the target.

B. Implementation Framework

The above discussion is based on a MDP model of vehicles. However, to deploy this approach in a real car, we need to abstract an MDP model from vehicle dynamics, as well as determine how to implement high-level policies obtained by solving the LP problem. The complete framework for implementation on autonomous vehicles is illustrated in Fig. 5. The related codes are available in [36].

Vehicle dynamics: In the experiments, we consider the dynamics of vehicles with a discrete-time bicycle model. Specifically, the system state consists of the horizontal position, heading angle, and linear speed of the vehicle, denoted by $[p_x, p_y]$, θ , and v , respectively. The control inputs to the vehicle are steering angle and acceleration, denoted by ϕ and a . Consequently, the system state is $\mathbf{x}(t) = [p_x(t), p_y(t), \theta(t), v(t)]^T \in \mathbb{X} \subset \mathbb{R}^4$, and the system input is $\mathbf{u}(t) = [\phi(t), a(t)]^T \in \mathbb{U} \subset \mathbb{R}^2$, where \mathbb{X} and \mathbb{U} are state

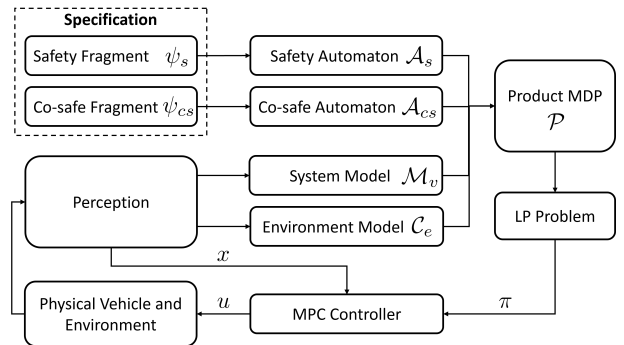


Fig. 5: The overall framework of control synthesis.

space and input space, respectively. The kinematic model of the vehicle is a bicycle model $\mathbf{x}(t+1) = f(\mathbf{x}(t), \mathbf{u}(t))$ of which the details can be referred to in [37]. To capture the environmental uncertainty, a zero-mean Gaussian-distributed disturbance vector, $\mathbf{w} \sim \mathcal{N}(0, \Sigma)$, is considered with the variance $\Sigma \in \mathbb{R}^{4 \times 4}$. The vehicle model with uncertainty is denoted by $\mathbf{x}(t+1) = f(\mathbf{x}(t), \mathbf{u}(t)) + \mathbf{w}(t)$.

From continuous dynamics to MDP: To abstract \mathcal{M}_v from the vehicle dynamics model with uncertainty, we first discretize the state space \mathbb{X} by gridding, where the finite state set S comprises the centers of the grid cells. For simplicity, this implementation considers only the horizontal positions of vehicles in \mathcal{M}_v . Similarly, the continuous input space \mathbb{U} is discretized into a finite action set A using appropriate interface functions. In this implementation, the transition probabilities are predefined by experts, which can also be generated autonomously and formally [19]. Additionally, the set of atomic propositions AP is determined by corresponding propositions in specifications, and the labeling function \mathcal{L} can be extracted from the semantic maps in the perception module. Since perception is beyond the scope of this paper, the labels are manually assigned in this implementation.

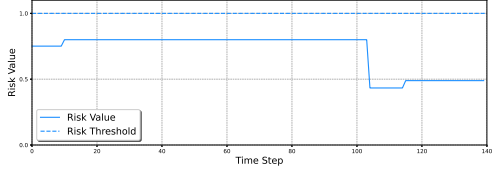
Control refinement: By solving the LP problem in Eq. (13), an optimal policy, π for \mathcal{M}_v , is obtained such that the next action can be determined according to π . To track the reference state denoted by $\mathbf{x}_r \in \mathbb{X}$ corresponding to the next action, a model predictive controller (MPC) is designed to drive the dynamic model of vehicles, formulated as follows,

$$\begin{aligned} \min_{\{\mathbf{u}_k\}_{k=0}^{N-1}} \quad & \sum_{k=0}^{N-1} (\mathbf{x}_{k+1} - \mathbf{x}_r)^T \mathbf{Q} (\mathbf{x}_{k+1} - \mathbf{x}_r) + \mathbf{u}_k^T \mathbf{R} \mathbf{u}_k \\ \text{s.t.} \quad & \mathbf{x}_{k+1} = f(\mathbf{x}_k, \mathbf{u}_k), \quad \mathbf{x}_0 = X_0, \\ & \mathbf{x}_{k+1} \in \mathbb{X}, \quad \mathbf{u}_k \in \mathbb{U}, \quad k=0, \dots, N-1, \end{aligned} \quad (14)$$

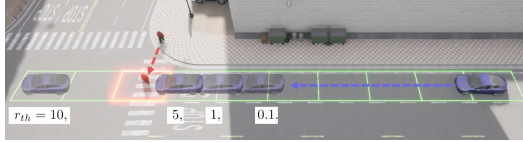
where N denotes a horizon number, X_0 is the current state, $\mathbf{Q} \in \mathbb{R}^{4 \times 4}$ and $\mathbf{R} \in \mathbb{R}^{2 \times 2}$ are diagonal weight matrixes. The first optimal control input is deployed to the vehicle.

C. Pedestrian Crossing Example

We first consider a simple scenario with a dynamic environment where a pedestrian is crossing at a crosswalk. The ego vehicle is expected to respond appropriately to the pedestrian's crossing behavior. To this end, we build an MC model to represent the uncertain behavior of the pedestrian. The specification of the ego vehicle is $\square(p \rightarrow$



(a) Risk curve for $r_{th}=1$



(b) Stopping points for different risk thresholds.

Fig. 6: Pedestrian crossing scenario

$\neg c \wedge \Diamond(t)$, where c and t denote the crosswalk and target zone respectively, and p represents the presence of a pedestrian on the crosswalk. The cost of hitting a pedestrian is set to 8. The ego vehicle is expected to autonomously decide whether to stop or proceed based on the real-time situation. From the risk curve shown in Fig. 6(a), the LP problem in Eq. (13) ensures that the risk always remains below the threshold. To test risk sensitivity, we set different risk thresholds r_{th} for the LP problem. The simulation results, depicted in Fig. 6(b), indicate that the ego vehicle will stop at a smaller clearance ahead of the crosswalk as the increase of risk threshold, i.e., $r_{th} = 0.1, 1, 5$. But $r_{th} = 10$ is too high to make the ego car account for the collision risk such that the ego car directly hits the pedestrian, which is undesirable. This result demonstrates the parameter r_{th} can be used to tune the conservatism of the synthesized policy.

In more complex scenarios, the LP problem encounters infeasibility in risky states, requiring a larger r_{th} . But a larger r_{th} will lead to unreasonably aggressive behavior in less risky states. As a result, while the formulation in (13) performs well in the pedestrian scenario, it generates unreasonable behavior in complex scenarios, such as unprotected turns in Fig. 1, which cannot be resolved by simply adjusting r_{th} . To address this issue, we propose an improved method in the next section.

V. IMPROVED RISK-AWARE CONTROL AND EXPERIMENTAL STUDY

Ideally, human drivers can actively minimize real-time risks while avoiding not only catastrophic outcomes but also overly conservative behavior. To achieve such a multi-objective balance, we introduce a soft risk threshold r_s and a hard risk threshold r_h to manage risk at different levels. This gives the following improved risk-aware control synthesis problem written as an LP optimization,

$$\begin{aligned} \max_{\{\beta_{\bar{\pi}}(z,a)\}} \quad & \bar{\mathcal{V}}_{\bar{\pi}}(\Diamond G) - K\xi \\ \text{s.t.} \quad & \sum_{z \in Z} \sum_{a \in A} c(z) \beta_{\bar{\pi}}(z,a) \leq r_s + \xi, \\ & \xi + r_s \leq r_h, \xi \geq 0, \\ & \beta_{\bar{\pi}}(z,a) \geq 0, \forall (z,a) \in Z \times A, \\ & \beta_{\bar{\pi}}(z') = (10), \forall z' \in Z, \end{aligned} \quad (15)$$

where ξ denotes the relaxation variable for soft risk threshold r_s and $K > 0$ is a constant to balance satisfying the co-safety specifications and minimizing the risks of safety specifications. The risk metric is minimized only when the target term forces the risk to exceed the soft threshold. Therefore, r_s filters out overly conservative behavior, while r_h ensures critical safety.

A. Experimental Study

We validate the improved risk-aware framework in three different scenarios, using default parameters: risk thresholds $r_s = 1$ and $r_h = 2$, and discounting factor $\gamma = 0.8$. The related video demonstration is accessible at the link ¹.

1) Pedestrian crossing scenario: The improved method ensures safety and generates behavior with tunable conservatism under the same settings as in Sec. IV-C, demonstrating that the improved LP problem encompasses functionalities of the original one in (13). The maximum and average risk values in the process are listed in Table I.

2) Unexpected construction scenario: Real-world traffic frequently encounters unexpected situations that make the original specifications infeasible [38], such as traffic participants violating rules or disruptions of traffic environments. We tested the proposed methods in such a scenario where an unexpected construction zone appears in the forward lane of the ego car, as illustrated in Fig. 7. In this case, the ego vehicle must deviate from a part of the original safety specifications to reach its target. The specification of this scenario for the ego vehicle is $\square(\neg c \wedge \neg o \wedge \neg s) \wedge \Diamond(t)$, where c, o, s and t are labels for construction areas, opposite lanes, sidewalks, and target areas. We assign cost values of 5, 3, and 1 to the construction area, sidewalk, and opposite lane, respectively. Figure 7 shows the generated trajectory, where the ego vehicle autonomously chooses to bypass the construction zone via the opposite lane with minimal violation and finally reaches the target. This result demonstrates that the improved control method effectively balances different risks and minimizes violations. This advantage arises from incorporating severity into LTL specifications.

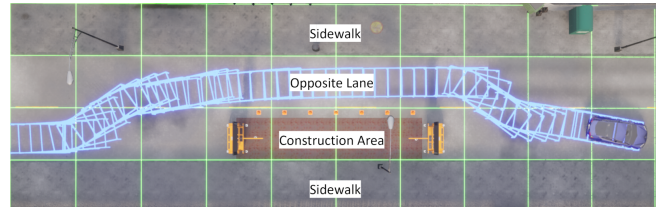


Fig. 7: The generated minimal-violation trajectory.

3) Unprotected turn scenario: We consider a complex intersection scenario that includes a traffic light system and dynamic opponent vehicles, as depicted in Fig. 1. The ego vehicle (blue car) is expected to follow traffic signals and avoid both non-drivable areas and the opponent vehicles (red car). The specification has been introduced in the study case of Sec. II-B. An MC model is designed to represent the

¹<https://youtu.be/r5kEMW8oPQE>

switching of traffic lights and the movement of the opponent vehicle. For simplicity, we assume the opponent vehicle always moving forward. The collision risk with the opponent vehicle is evaluated by calculating the overlap between risk fields of vehicles, following the method described in [24]. With the policy synthesized by the LP problem, the ego vehicle will wait at the boundary of the intersection until the light turns green, adjust its decisions based on the real-time positions of the opponent vehicles, and finally reach the target position. The whole process is illustrated in Fig. 1 and the attached video. This case accounts for traffic lights, non-drivable areas, and other dynamic vehicles, which are typical factors in traffic. Thus, this method can handle complex situations and has the potential to scale to various scenarios.

To examine the influence of different discounting factors, the corresponding risk curves are shown in Fig. 8. While the generated behavior remains identical across different discounting factors, the risk curves in the process are different. Compared to $\gamma = 0.8$, the discounting factor $\gamma = 0.5$ places more emphasis on recent events, causing the risk curves of $\gamma = 0.5$ to gradually increase as the two vehicles approach each other. In contrast, the risk curves for $\gamma = 0.8$ remain flatter because the encounter is perceived earlier. Since placing more focus on recent events lowers perceived risk values, the thresholds are adjusted accordingly.

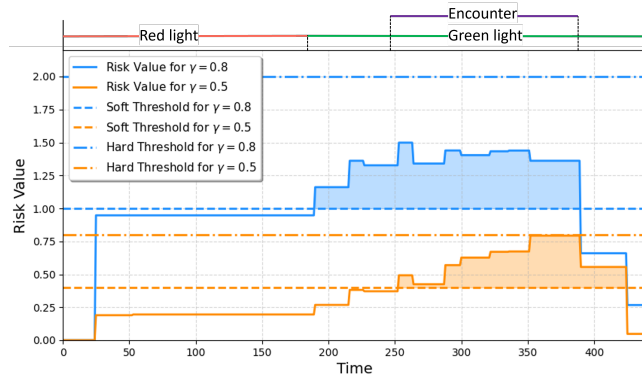


Fig. 8: Risk curves under different discounting factors.

Table I presents the maximum and average risk values with the default discounting and threshold, along with the state number and computation time for the LP problem in (13). The results show that the improved LP problem effectively manages different types of risk and maintains gross risk value within the predefined level throughout the execution process. However, computation time increases significantly as the number of states grows such that a coarse abstraction is adopted. Future work will explore adaptive abstraction and approximation methods to improve computational efficiency.

	Scenario 1	Scenario 2	Scenario 3
Maximal risk	0.8	1.46	1.51
Average risk	0.68	0.97	1.01
State number	1440	720	2880
Computation time/ms	20-30	15-20	50-60

TABLE I: Risk value and computation time in the three scenarios.

VI. CONCLUSION

In this paper, we extend a human-like risk metric to account for complex traffic scenarios by integrating LTL specifications. On the other hand, the proposed metric enhances the practicality of temporal logic in traffic tasks by incorporating human-like awareness. Furthermore, a risk-aware control method is improved to balance different types of risks in a human-like manner. Extensive simulation results validate the effectiveness and potential of this framework and illustrate the impact of various parameters. To better handle realistic traffic, future work should incorporate strategic interactions between vehicles, reduce computational costs for finer abstractions, and learn parameters from real-road data instead of manual configuration.

REFERENCES

- [1] N. Mehdipour, M. Althoff, R. D. Tebbens, and C. Belta, “Formal methods to comply with rules of the road in autonomous driving: State of the art and grand challenges,” *Automatica*, vol. 152, p. 110692, 2023.
- [2] W. Wang, L. Wang, C. Zhang, C. Liu, L. Sun, *et al.*, “Social interactions for autonomous driving: A review and perspectives,” *Foundations and Trends® in Robotics*, vol. 10, no. 3-4, pp. 198–376, 2022.
- [3] I. Hasuo, “Responsibility-sensitive safety: an introduction with an eye to logical foundations and formalization,” *arXiv preprint arXiv:2206.03418*, 2022.
- [4] S. Maierhofer, P. Moosbrugger, and M. Althoff, “Formalization of intersection traffic rules in temporal logic,” in *2022 IEEE Intelligent Vehicles Symposium (IV)*, pp. 1135–1144, IEEE, 2022.
- [5] I. Nastjuk, B. Herrenkind, M. Marrone, A. B. Brendel, and L. M. Kolbe, “What drives the acceptance of autonomous driving? an investigation of acceptance factors from an end-user’s perspective,” *Technological Forecasting and Social Change*, vol. 161, p. 120319, 2020.
- [6] J. Li, D. Isele, K. Lee, J. Park, K. Fujimura, and M. J. Kochenderfer, “Interactive autonomous navigation with internal state inference and interactivity estimation,” *IEEE Transactions on Robotics*, vol. 40, pp. 2932–2949, 2024.
- [7] T. Wongpiromsarn, K. Slutsky, E. Frazzoli, and U. Topcu, “Minimum-violation planning for autonomous systems: Theoretical and practical considerations,” in *2021 American Control Conference (ACC)*, pp. 4866–4872, IEEE, 2021.
- [8] A. Censi, K. Slutsky, T. Wongpiromsarn, D. Yershov, S. Pendleton, J. Fu, and E. Frazzoli, “Liability, ethics, and culture-aware behavior specification using rulebooks,” in *2019 International Conference on Robotics and Automation (ICRA)*, pp. 8536–8542, IEEE, 2019.
- [9] C. Belta, B. Yordanov, and E. A. Gol, *Formal methods for discrete-time dynamical systems*, vol. 89. Springer, 2017.
- [10] L. Lindemann and D. V. Dimarogonas, “Control barrier functions for signal temporal logic tasks,” *IEEE control systems letters*, vol. 3, no. 1, pp. 96–101, 2018.
- [11] S. Qi, Z. Zhang, S. Haesaert, and Z. Sun, “Automated formation control synthesis from temporal logic specifications,” in *2023 62nd IEEE Conference on Decision and Control (CDC)*, pp. 5165–5170, IEEE, 2023.
- [12] S. Maierhofer, A.-K. Rettinger, E. C. Mayer, and M. Althoff, “Formalization of interstate traffic rules in temporal logic,” in *2020 IEEE Intelligent Vehicles Symposium (IV)*, pp. 752–759, IEEE, 2020.
- [13] C. Belta and S. Sadraddini, “Formal methods for control synthesis: An optimization perspective,” *Annual Review of Control, Robotics, and Autonomous Systems*, vol. 2, no. 1, pp. 115–140, 2019.
- [14] T. Wongpiromsarn, M. Ghasemi, M. Cubuktepe, G. Bakirtzis, S. Carr, M. O. Karabag, C. Neary, P. Gohari, and U. Topcu, “Formal methods for autonomous systems,” *arXiv preprint arXiv:2311.01258*, 2023.
- [15] M. Guo and M. M. Zavlanos, “Probabilistic motion planning under temporal tasks and soft constraints,” *IEEE Transactions on Automatic Control*, vol. 63, no. 12, pp. 4051–4066, 2018.
- [16] L. Lindemann, N. Matni, and G. J. Pappas, “Stl robustness risk over discrete-time stochastic processes,” in *2021 60th IEEE Conference on Decision and Control (CDC)*, pp. 1329–1335, IEEE, 2021.

- [17] S. S. Farahani, R. Majumdar, V. S. Prabhu, and S. Soudjani, “Shrinking horizon model predictive control with signal temporal logic constraints under stochastic disturbances,” *IEEE Transactions on Automatic Control*, vol. 64, no. 8, pp. 3324–3331, 2018.
- [18] S. Haesaert and S. Soudjani, “Robust dynamic programming for temporal logic control of stochastic systems,” *IEEE Transactions on Automatic Control*, vol. 66, no. 6, pp. 2496–2511, 2020.
- [19] B. C. van Huijgevoort, S. Weiland, and S. Haesaert, “Temporal logic control of nonlinear stochastic systems using a piecewise-affine abstraction,” *IEEE Control Systems Letters*, vol. 7, pp. 1039–1044, 2022.
- [20] L. Lindemann, G. J. Pappas, and D. V. Dimarogonas, “Reactive and risk-aware control for signal temporal logic,” *IEEE Transactions on Automatic Control*, vol. 67, no. 10, pp. 5262–5277, 2021.
- [21] M. Geisslinger, F. Poszler, J. Betz, C. Lütge, and M. Lienkamp, “Autonomous driving ethics: From trolley problem to ethics of risk,” *Philosophy & Technology*, vol. 34, no. 4, pp. 1033–1055, 2021.
- [22] M. H. W. Engelaar, Z. Zhang, M. Lazar, and S. Haesaert, “Risk-aware mpc for stochastic systems with runtime temporal logics,” *arXiv preprint arXiv:2402.03165*, 2024.
- [23] S. Kolekar, J. de Winter, and D. Abbink, “Human-like driving behaviour emerges from a risk-based driver model,” *Nature Communications*, vol. 11, no. 1, p. 4850, 2020.
- [24] Y.-J. Joo, E.-J. Kim, D.-K. Kim, and P. Y. Park, “A generalized driving risk assessment on high-speed highways using field theory,” *Analytic methods in accident research*, vol. 40, p. 100303, 2023.
- [25] A. Artale, L. Geatti, N. Gigante, A. Mazzullo, and A. Montanari, “Complexity of safety and cosafety fragments of linear temporal logic,” in *Proceedings of the AAAI Conference on Artificial Intelligence*, vol. 37, pp. 6236–6244, 2023.
- [26] E. Altman, *Constrained Markov decision processes*. Routledge, 2021.
- [27] S. Haesaert, P. Nilsson, and S. Soudjani, “Formal multi-objective synthesis of continuous-state mdps,” in *2021 American Control Conference (ACC)*, pp. 3428–3433, IEEE, 2021.
- [28] A. Dosovitskiy, G. Ros, F. Codevilla, A. Lopez, and V. Koltun, “Carla: An open urban driving simulator,” in *Conference on robot learning*, pp. 1–16, PMLR, 2017.
- [29] M. J. Kochenderfer, *Decision making under uncertainty: theory and application*. MIT press, 2015.
- [30] A. Ulusoy, T. Wongpiromsarn, and C. Belta, “Incremental controller synthesis in probabilistic environments with temporal logic constraints,” *The International Journal of Robotics Research*, vol. 33, no. 8, pp. 1130–1144, 2014.
- [31] J. G. Henriksen, J. Jensen, M. Jørgensen, N. Klarlund, R. Paige, T. Rauhe, and A. Sandholm, “Mona: Monadic second-order logic in practice,” in *Tools and Algorithms for the Construction and Analysis of Systems: First International Workshop, TACAS’95 Aarhus, Denmark, May 19–20, 1995 Selected Papers 1*, pp. 89–110, Springer, 1995.
- [32] A. Majumdar and M. Pavone, “How should a robot assess risk? towards an axiomatic theory of risk in robotics,” in *Robotics Research: The 18th International Symposium ISRR*, pp. 75–84, Springer, 2020.
- [33] A. Ahmed, “Rationality and future discounting,” *Topoi*, vol. 39, no. 2, pp. 245–256, 2020.
- [34] F. Trevizan, S. Thiébaut, and P. Haslum, “Occupation measure heuristics for probabilistic planning,” in *Proceedings of the International Conference on Automated Planning and Scheduling*, vol. 27, pp. 306–315, 2017.
- [35] Gurobi Optimization, LLC, “Gurobi Optimizer Reference Manual,” 2024.
- [36] S. Qi, “Risk LTL planning,” *GitHub*, 2024. Available at https://github.com/Miracle-qi/Risk_LTL_Planning.
- [37] Z. Zhang, Z. Sun, and S. Haesaert, “Intention-aware control based on belief-space specifications and stochastic expansion,” *IEEE Transactions on Intelligent Vehicles*, 2024.
- [38] J. Tůmová, L. I. Reyes Castro, S. Karaman, E. Frazzoli, and D. Rus, “Minimum-violation ltl planning with conflicting specifications,” in *2013 American Control Conference*, pp. 200–205, 2013.